THE JOURNAL OF BIOLOGICAL CHEMISTRY VOL. 285, NO. 52, pp. 41100–41112, December 24, 2010

A Conserved Protein Interaction Interface on the Type 5 G Protein β Subunit Controls Proteolytic Stability and Activity of R7 Family Regulator of G Protein Signaling Proteins*[S]

Received for publication, July 12, 2010 and in revised form, October 19, 2010 Published, JBC Papers in Press, October 19, 2010, DOI 10.1074/jbc.M110.163600

Morwenna Y. Porter[‡1,2], **Keqiang Xie**[§1], **Edwin Pozharski**[¶], **Michael R. Koelle**[‡3], **and Kirill A. Martemyanov**[§4]

From the [§]*Department of Pharmacology, University of Minnesota, Minneapolis, Minnesota 55455, the* [‡]*Department of Molecular Biophysics and Biochemistry, Yale University School of Medicine, New Haven, Connecticut 06520, and the* [¶]*Department of Pharmaceutical Sciences, University of Maryland School of Pharmacy, Baltimore, Maryland 21201*

Regulators of G protein signaling (RGS) proteins of the R7 subfamily limit signaling by neurotransmitters in the brain and by light in the retina. They form obligate complexes with the Gβ5 protein that are subject to proteolysis to control their abundance and alter signaling. The mechanisms that regulate this proteolysis, however, remain unclear. We used genetic screens to find mutations in Gβ5 that selectively destabilize one of the R7 RGS proteins in *Caenorhabditis elegans*. These mutations cluster at the binding interface between Gβ5 and the N terminus of R7 RGS proteins. Equivalent mutations within mammalian Gβ5 allowed the interface to still bind the N-terminal DEP domain of R7 RGS proteins, and mutant Gβ5-R7 RGS complexes initially formed in cells but were then rapidly degraded by proteolysis. Molecular dynamics simulations suggest the mutations weaken the Gβ5-DEP interface, thus promoting dynamic opening of the complex to expose determinants of proteolysis known to exist on the DEP domain. We propose that conformational rearrangements at the Gβ5-DEP interface are key to controlling the stability of R7 RGS protein complexes.

G protein pathways are ubiquitous signaling systems that provide control over virtually all cellular functions (1, 2). The duration and extent of signaling in these pathways are critically shaped by the regulator of G protein signaling (RGS)[5] proteins, consisting over 30 members (3, 4). In the nervous systems, a key role in the regulation of neurotransmitter signaling belongs to the R7 family of RGS proteins. Members of this protein family are conserved throughout the animal kingdom and regulate fundamental neuronal functions ranging from egg laying behavior and locomotion in *Caenorhabditis elegans* (5, 6) to vision, nociception, motor coordination, and reward behavior in mammals (7).

Four mammalian R7 RGS proteins (RGS6, RGS7, RGS9, and RGS11) act preferentially to speed up the inactivation of the $G_{i/o}$ class of Gα proteins activated by rhodopsin, D_2 dopamine, μ-opioid, and other receptors (reviewed in Ref. 7). Inactivation of R7 RGS proteins in mice leads to visual defects, motor coordination deficits, and enhanced effects of addictive drugs (7, 8). In *C. elegans*, two ancestral R7 RGS proteins, EGL-10 and EAT-16, inhibit $G\alpha_o$ and $G\alpha_q$ proteins, respectively (Fig. 1*A*), to antagonistically control egg laying, locomotion, and other behaviors (5, 6).

Both mammalian and *C. elegans* R7 RGS proteins share considerable sequence similarity and a common domain organization. In addition to the RGS homology domain that acts as a GTPase activator to terminate Gα signaling, these proteins possess an N-terminal DEP/DHEX (disheveled/EGL-10/pleckstrin similarity domain/DEP helical extension) module that recruits the soluble NSF attachment protein receptor-like membrane-binding protein R7BP/RSBP-1, followed by the GGL (G gamma-like) domain that binds the atypical G protein β subunit Gβ5/GBP-2 (6, 7, 9). Association with Gβ5/GBP-2 and R7BP/RSBP-1 is essential for the stability of these complexes. Although disruption of R7BP/RSBP-1 selectively destabilizes RGS9 and EAT-16 (9, 10), knock-out of Gβ5/GBP-2 essentially eliminates the expression of all R7 RGS proteins (11, 12) leading to the hypothesis that interactions with Gβ5 play a central role in controlling the stability of R7 RGS proteins. The recent crystal structure of the RGS9·Gβ5 complex indicates that Gβ5 has three distinct interactions with R7 proteins as follows: in addition to marginal contacts with the RGS domain, it forms extensive contacts with the GGL and the DEP domains (13).

Alterations to R7 RGS protein levels are thought to be an important mechanism underlying signaling plasticity and have been documented in response to changes in receptor activation status under pathological conditions such as Parkinson disease (14) and addiction (15, 16). Experiments in *C. elegans* (9, 17) and mice (16, 18, 19) indicate that the abundance of R7 RGS proteins is critically important in determin-

* This work was supported, in whole or in part, by National Institutes of Health Grants EY018139 (to K. A. M.), DA021743 (to K. A. M.), DA026405 (to K. A. M.), NS036918 (to M. R. K.), and MH082201 (to M. R. K.). This work was also supported by the McKnight Land Grant Professorship (to K. A. M.).

[S] The on-line version of this article (available at http://www.jbc.org) contains supplemental Fig. 1 and Tables 1 and 2.

[1] Both authors contributed equally to this work and are listed alphabetically.

[2] Present address: Astbury Centre for Structural Molecular Biology, Institute of Molecular and Cellular Biology, University of Leeds, Leeds LS2 9JT, United Kingdom.

[3] To whom correspondence may be addressed: Dept. of Molecular Biophysics and Biochemistry, Yale University School of Medicine, 333 Cedar St., New Haven, CT 06520. Tel.: 203-737-5808; Fax: 203-785-7979; E-mail: michael.koelle@yale.edu.

[4] To whom correspondence may be addressed: Dept. of Pharmacology, University of Minnesota, 6-120 Jackson Hall, 321 Church St. SE, Minneapolis, MN 55455. Tel.: 612-626-5309; Fax: 612-625-8408; E-mail: martemyanov@umn.edu.

[5] The abbreviations used are: RGS, regulators of G protein signaling; MD, molecular dynamics.

ing the extent of their regulatory influence. The mechanisms that alter R7 RGS abundance remain unclear, but any mechanism that dynamically regulates protein abundance requires protein turnover. Given the sensitivity of R7 RGS proteins to degradation, their turnover may in fact be the regulated step.

In this study, we have used the power of *C. elegans* genetics to identify an unusual mutation in Gβ5/GBP-2 that preferentially affects the stability of EAT-16 over EGL-10, resulting in a characteristic hyperactive phenotype caused by enhanced $G\alpha_q$ signaling. Interestingly, previous genetic screens reported several mutations in Gβ5/GBP-2 with similar functional properties but unexplained mechanisms (20, 21). Our analysis shows that all of the identified "hyperactive" mutations are in residues conserved in mammals and disrupt the Gβ5-DEP interface, which serves as the hot spot for the regulation of complex stability.

EXPERIMENTAL PROCEDURES

Nematode Strains and Culture—*C. elegans* strains were maintained and double mutants generated using standard techniques (22). All strains used are listed in supplemental Table 1, and all *gpb-2* mutations are listed in supplemental Table 2. *vs33* was isolated in a screen for hyperactive egg-laying mutants (23, 24) and mapped using standard genetic techniques. Briefly, single nucleotide polymorphism mapping (25) placed *vs33* between −0.69 and 5.06 centimorgans on the genetic map of chromosome I. A combination of three-factor mapping and single nucleotide polymorphism analysis further positioned *vs33* between two visible markers at 0.00 (*dpy-5*) and 3.30 (*unc-29*). Subsequent sequencing of candidate G protein signaling genes within this region identified a 3-bp deletion in *gpb-2* that eliminates the Asp-263 codon.

C. elegans Behavior and Morphology—Egg laying assays were performed as described previously (26). To determine the number of unlaid eggs, adult animals were dissolved in bleach and the number of bleach-resistant eggs counted. To determine the percentage of eggs laid at each developmental stage, adult animals were allowed to lay eggs for 30 min, and the eggs were visually inspected. In the unlaid egg assay, 30 animals per genotype were analyzed, and the mean and 95% confidence intervals were calculated. In the developmental stage assay, ≥100 eggs per strain were analyzed, and 95% confidence intervals and *p* values were calculated using Wilson's estimates. Precisely staged adults for both assays were obtained by isolating late L4 larvae and aging for 30 h at 20 °C.

To qualitatively analyze locomotion and foraging, individual worms were filmed moving across a bacterial lawn with a digital video camera attached to a Leica M420 dissecting microscope. Tracks were traced manually. To visualize morphology, worms were imaged on a Zeiss Axioskop microscope.

DNA Constructs and Site-directed Mutagenesis—Cloning of full-length Gβ5, R7BP, RGS7, and RGS9-2 was described previously (27). To generate N-terminal HA-tagged RGS7 (HA-RGS7), the RGS7 cDNA was cloned into the pCMV-HA vector. Gβ5-D260A, Gβ5-C263Y, and Gβ5-D304N mutants were generated using the single site-directed mutagenesis kit (Stratagene) following the manufacturer's instructions. The following paired primers were used for site-directed mutagenesis: Gβ5D260A (sense), 5′-GCTTCGGGGTCGGATGCAGCCACGTGTCGCCTC, and Gβ5D260A (antisense), 5′-GAGGCGACACGTGGCTGCATCCGACCCCGAAGC; Gβ5C263Y (sense), 5′-TCGGATGATGCCACGTATCGCCTCTATGACCTG, and Gβ5C263Y (antisense), 5′-CAGGTCATAGAGGCGATACGTGGCATCATCCGA; Gβ5D304N (sense), 5′-TTTGCTGGGTACAATAACTATACCATCAATGTC, and Gβ5D304N (antisense) 5′-GACATTGATGGTATAGTTATTGTACCCAGCAAA. The N-terminal AU5-tagged Gβ5 wild-type and mutant (AU5-Gβ5, AU5-Gβ5D260A, and AU5-Gβ5C263Y) fragments were amplified with AU5-Gβ5 (sense), 5′-ATGACAGACTTTTACCTCAAAGCAACCGATGGGCTGCAC, and Gβ5 (antisense), 5′-TTATGCCCAAACTCTTAGGG paired primers. The N-terminal fragment of RGS9 (amino acids 1–209) with c-myc tag at the C terminus was amplified using the following paired primers: RGS9 (sense), 5′-ATGACGATCCGACACCAAGG, and RGS9 (antisense), 5′-TCACAGATCTTCTTCAGAAATAAGTTTTTGTTCCATGGTCACGCGGTCCAGGCCGT. The C-terminal fragment of RGS9-1 (amino acids 210–484) with HA tag at the C terminus was amplified using the following primers: RGS9CT (sense), 5′-ATGAATCCAAACGAAGTTAAGAA, and RGS9-1CTHA (antisense), 5′-TCAAGCGTAATCTGGAACATCGTATGGGTACATTTTAGGAGGCAGCTCCTTTTTG. All PCR products were cloned into the pcDNA3.1/V5-His-TOPO (Invitrogen) mammalian expression vector according to the manufacturer's specifications. Constructs were propagated in the *Escherichia coli* Top-10 strain (Invitrogen), isolated using Maxiprep kits (Qiagen), and sequenced. PhLP1 containing the C-terminal c-myc tag (pcDNA3.1) was kindly provided by Dr. Barry Willardson (Brigham Young University).

Cell Culture and Transfections—HEK293FT cells were cultured at 37 °C and 5% CO_2 in DMEM supplemented with antibiotics, 10% fetal bovine serum, and 4 mM L-glutamine. Cells were transfected at 70% confluency using Lipofectamine LTX reagent (Invitrogen) according to the manufacturer's protocol. The cells were grown for 24–48 h post-transfection.

Cell Lysis, Immunoprecipitation, and Western Blotting—*C. elegans* liquid cultures were grown at 20 °C and isolated by flotation on 30% sucrose. Packed worm pellets were resuspended in lysis buffer (50 mM HEPES, 100 mM NaCl, 1 mM PMSF, 1 μg/ml leupeptin, 1 μg/ml pepstatin) and lysed either by sonication (pellets ≤0.5 ml), as described previously (9), or passaged three times through a French press at 800 p.s.i. (pellets ≥0.5 ml). Debris was removed by centrifugation at 800 × *g* for 10 min at 4 °C. Protein concentrations were determined by the Bio-Rad protein assay using BSA as a standard.

Mammalian cells from 1 well of a 6-well plate were lysed in 500 μl of PBS buffer supplemented with 150 mM NaCl, 1% Triton X-100, and Complete protease inhibitor (Roche Applied Science). The homogenate was centrifuged at 15,000 × *g* for 15 min at 4 °C.

For the immunoprecipitation, supernatants were incubated with a specific antibody as indicated, and 20 μl of 50% protein G slurry (GE healthcare) on a rocker at 4 °C for 1 h. After three washes with lysis buffer, proteins were eluted from beads with 50 μl of SDS sample buffer by boiling for 5 min.

Proteins in the eluates were separated by SDS-PAGE, transferred to nitrocellulose or PVDF membranes, and probed with the indicated specific primary antibodies followed by secondary antibodies coupled to horseradish peroxidase. Signals were detected using West Pico enhanced chemiluminescence system (Pierce). The following primary antibodies were used: sheep anti-RGS9-2, rabbit anti-RGS7 (7RC1), rabbit anti-Gβ5 (ATDG), anti-c-Myc (GenScript); anti-HA (Millipore); anti-AU5 (MMS-135R, Covance); anti-CCTϵ (MCA2178, AbD Serotec); anti-PhLP1 (kindly provided by Dr. Barry Willardson); rabbit anti-EGL-10 (17); rabbit anti-EAT-16 (9); rabbit anti-GPB-2 (12); rabbit anti-UNC-64/Syntaxin (a kind gift from M. Nonet, Washington University); and mouse anti-β-tubulin (E7, DSHB, University of Iowa).

Pulse-Chase Degradation Experiments—Experiments to evaluate the stability of RGS proteins to proteolytic degradation were performed in HEK293FT cells as described previously (28). HEK293FT cells grown in T-25 flasks were transfected with RGS constructs with or without wild-type or mutant Gβ5 constructs. For assays involving RGS9, R7BP was additionally co-transfected. Total cDNAs were 5 μg per flask. Twenty four hours after transfection, the cells were rinsed twice with PBS, placed into 5 ml of starvation medium (10% dialyzed fetal bovine serum (Invitrogen), DMEM without L-methionine or L-cysteine (21013-024, Invitrogen)), and incubated at 37 °C and 5% CO_2 for 30 min. Subsequently, newly synthesizing proteins were labeled by adding 175 μCi of [^{35}S]methionine/cysteine (NEG772; PerkinElmer Life Sciences) per flask to the starvation medium and incubating at 37 °C for 40 min. Cells were rinsed twice with 2 ml of DMEM and incubated with 5 ml of complete medium supplemented by additional 2 mM L-methionine and 2 mM L-cysteine (Sigma) at 37 °C for the indicated incubation times. At the end of the incubation, the cells were scraped into 5 ml of ice-chilled PBS, pelleted by centrifugation, and resuspended in 900 μl of radioimmune precipitation assay buffer (50 mM Tris-HCl, pH 7.8, 300 mM NaCl, 1 mM EDTA, 1% Triton X-100, 0.5% sodium deoxycholate, 0.1% SDS) supplemented with protease inhibitors (Complete; Roche Applied Science). After 20 min of incubation at 4 °C, the suspension was then centrifuged at 4 °C and 14,000 × *g* for 30 min, and the resulting supernatant was incubated with 20 μl of protein G beads slurry and 3 μg of RGS9-2 CT antibody or HA antibody for 1 h at 4 °C. After three washes, immunoprecipitated proteins were eluted from the beads by 50 μl of SDS sample buffer. Samples were run on SDS-PAGE and transferred to a PVDF membrane (Bio-Rad). The membrane was air-dried and incubated on a phosphorimaging screen overnight. This screen was then scanned using a STORM phosphorimager (GE Healthcare), and the bands were quantified using ImageQuant software (GE Healthcare). Each experiment was repeated at least twice.

Recombinant Proteins—RGS7, RGS9-2, and wild-type Gβ5 recombinant baculoviruses were described previously (29, 30). Mutant Gβ5 constructs (Gβ5-D260A and Gβ5-C263Y) were used to generate recombinant baculoviruses using the BaculoDirect C-terminal expression kit (Invitrogen) following the manufacturer's manual. Proteins were expressed in Sf-9 cells, and protein complexes were purified by nickel-nitrilotriacetic acid chromatography taking advantage of the His tag engineered at the N terminus of RGS proteins as described previously (29). Recombinant GST-tagged R7BP protein was expressed in *E. coli* and purified as described previously (30).

GST Pulldown Assay—The assays were performed as described previously (27). Briefly, purified recombinant GST fusion R7BP or GST control protein (0.25 μM) and purified R7 RGS-Gβ5 proteins (0.25 μM) were co-incubated with 20 μl of 50% glutathione-agarose bead slurry (GE Healthcare) in binding buffer (20 mM Tris, pH 7.2, 300 mM NaCl, 0.25% *n*-dodecanoylsucrose, 50 μg/ml bovine serum albumin) for 1 h at 4 °C. The beads were washed with binding buffer three times. Proteins were eluted in SDS sample buffer, and proteins present in the eluates were detected by immunoblotting with anti-RGS7 (7RC1), anti-Gβ5 (ATDG), and anti-R7BP (NT) antibodies.

In Silico Molecular Dynamic Simulations—Molecular dynamics simulations were performed using GROMACS (31). An identical procedure was used for all the models studied in this work and consisted of the following steps. A model with generated hydrogens was placed in a box of appropriate size and fully solvated. Protonation states of ionizable groups were assigned based on analysis of hydrogen bonding patterns. Sufficient numbers of sodium and chloride ions were placed in random positions to emulate physiological ionic strength (150 mM) and to neutralize the overall charge of the system. The fully solvated model was subjected to energy minimization followed by 20-ps simulation with protein atoms restrained to their positions in the crystal structure to allow water relaxation. Finally, 100-ps unrestrained simulation was performed at 300 K. Snapshots were obtained every 500 fs, and it was found that initial equilibration period did not exceed 30 ps (as judged by overall root mean square deviation of aligned models). The second half of the unrestrained simulation was used for analysis.

RESULTS

A Novel Allele of GPB-2/Gβ5 Causes Hyperactive Behavior in C. elegans—To further our understanding of the mechanisms that regulate G protein signaling, we performed a genetic screen for animals hyperactive for egg laying, a behavior controlled by R7 RGS·Gβ5 complexes (23). We identified a novel allele, *vs33,* and mapped it to a small interval on chromosome I containing the gene *gpb-2*/Gβ5. This mutation deletes the codon for aspartate 263 from this gene.

Wild-type animals hold their fertilized eggs *in utero* for a few hours while the embryos develop past the eight-cell stage. As a result, wild-type animals accumulate 9.1 ± 0.6 eggs *in utero* and lay only 12.3 ± 6.4% of their eggs at an early developmental stage of less than eight cells (Fig. 1*B*). Wild-type animals also move across a bacterial lawn in a sinusoidal wave, make few reversals, and forage over much of the available bacterial lawn (Fig. 1*C*). These behaviors are the result of a balance between the opposing effects of $G\alpha_o$ and $G\alpha_q$ signaling (Fig. 1*D*).

GPB-2/Gβ5 is an essential subunit of the two *C. elegans* R7 RGS proteins, EGL-10 and EAT-16, which inhibit $G\alpha_o$ and $G\alpha_q$ signaling, respectively (12, 20, 32). In animals lacking

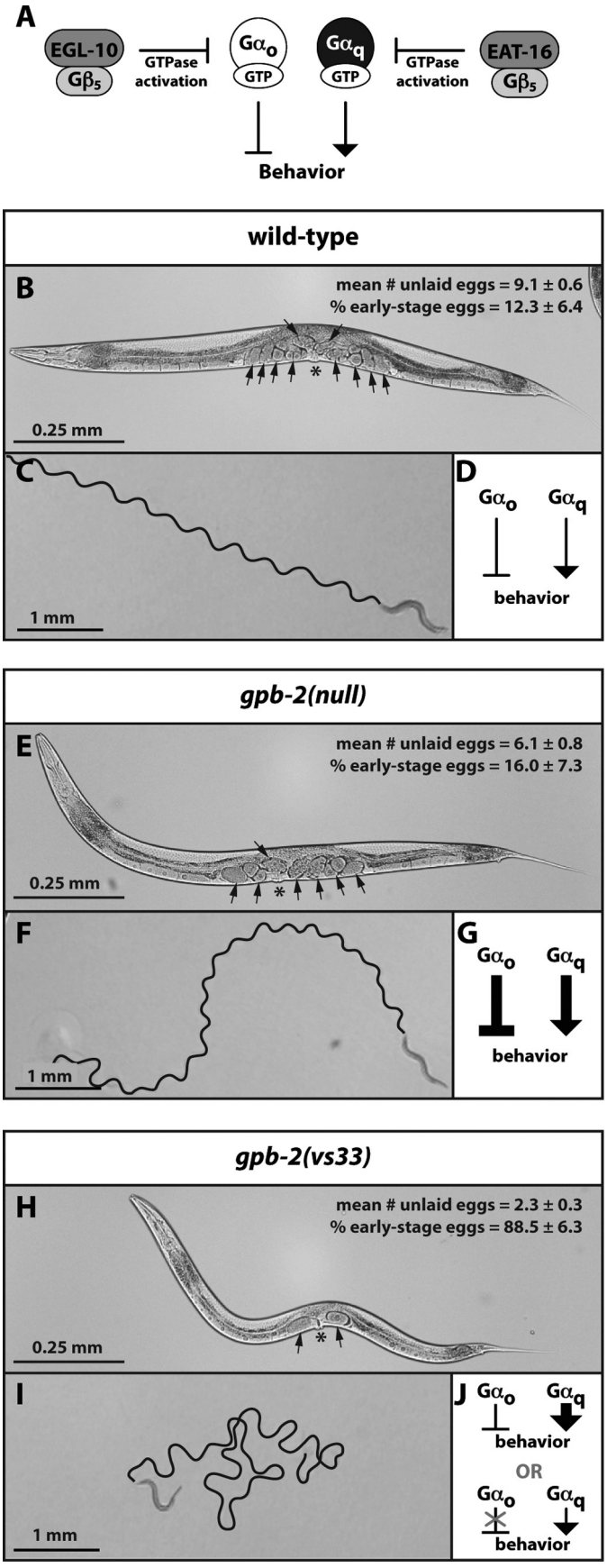

FIGURE 1. **Egg laying and locomotion behavior in wild-type animals, *gpb-2*(*null*) mutants, and *gpb-2*(*vs33*) animals.** *A,* diagram showing R7 RGS regulation of $G\alpha_o$ and $G\alpha_q$ signaling in *C. elegans*. *B, E,* and *H,* representative images of the indicated genotypes. The mean number of unlaid eggs and percentage early stage eggs laid ±95% confidence interval are indicated. *Arrows* mark unlaid eggs; *asterisks* mark the vulva. *C, F,* and *I,* representative images of tracks made by animals of the indicated genotypes crossing a bacterial lawn. *D, G,* and *J,* G protein signaling levels in animals of the indicated genotypes. *gpb-2*(*vs33*) animals exhibit hyperactive behavior due to either increased $G\alpha_q$ signaling or decreased $G\alpha_o$ signaling.

GPB-2/Gβ5, there is no inhibition of $G\alpha_o$ or $G\alpha_q$, and signaling by both G proteins is increased (Fig. 1*G*). However, as this does not alter the net balance of signaling, *gpb-2*(*null*) mutants appear grossly wild type in appearance and behavior. Consistent with previously published data, we observed that *gpb-2*(*null*) mutants accumulate 6.1 ± 0.8 eggs *in utero*, lay only 16.0 ± 7.3% of their eggs at an early developmental stage (Fig. 1*E*), and exhibit locomotion and foraging behavior similar to that of wild-type animals (Fig. 1*F*).

In surprising contrast to *gpb-2*(*null*) mutants, we found that *gpb-2*(*vs33*) mutants are strongly hyperactive for egg laying and locomotion behaviors. *gpb-2*(*vs33*) animals lay their eggs almost as soon as they are fertilized and thus accumulate only 2.3 ± 0.3 unlaid eggs and lay 88.5 ± 6.3% of their eggs at an early developmental stage (Fig. 1*H*). In addition, *gpb-2*(*vs33*) mutants move with much deeper body bends than wild-type animals, make more reversals, and restrict their foraging to a smaller area of the bacterial lawn (Fig. 1*I*). *gpb-2*(*vs33*) mutants are also thin and pale compared with the wild-type or *gpb-2*(*null*) animals (Fig. 1, *B*, *E*, and *H*). Finally, whereas wild-type animals are paralyzed by exogenously applied serotonin and dopamine (26, 33), *gpb-2*(*vs33*) mutants but not *gpb-2*(*null*) animals are resistant to these effects (data not shown).

The defects exhibited by *gpb-2*(*vs33*) animals are characteristic of animals in which either signaling by the inhibitory G protein, $G\alpha_o$, is decreased or signaling by the stimulatory G protein, $G\alpha_q$, is increased (Fig. 1*J*). Interestingly, two other point mutations in *gpb-2*, the alleles *sa833* and *sa604*, have been reported to cause the very same set of defects as observed in the *gpb-2*(*vs33*) mutants (supplemental Table 2) (20). We have named these *gpb-2*(*hyp*) mutations.

$G\alpha_q$ Signaling Is Increased in gpb-2(hyp) Mutants—To determine whether the behavioral defects seen in *gpb-2*(*hyp*) mutants are the result of decreased $G\alpha_o$ signaling or increased $G\alpha_q$ signaling, we first took a genetic approach. We hypothesized that *gpb-2*(*hyp*) mutations may either increase EGL-10 activity, causing decreased inhibitory $G\alpha_o$ signaling, or may decrease EAT-16 activity, resulting in increased stimulatory $G\alpha_q$ signaling. To distinguish between these alternatives, we combined each *gpb-2*(*hyp*) mutation with a null allele of *egl-10.* If the *gpb-2*(*hyp*) mutations increase EGL-10 activity, then in the absence of EGL-10 they should have no effect, and the double mutants should phenocopy *egl-10*(*null*) single mutants. However, if *gpb-2*(*hyp*) mutants decrease EAT-16 activity, resulting in increased $G\alpha_q$ signaling, then in the absence of EGL-10, $G\alpha_o$ signaling will also be increased to restore the balance of signaling, as in *gpb-2*(*null*) mutants, so that the double mutants should resemble both wild-type and *gpb-2*(*null*) animals. We analyzed the stage of the eggs laid by each strain, and these data are presented in Fig. 2.

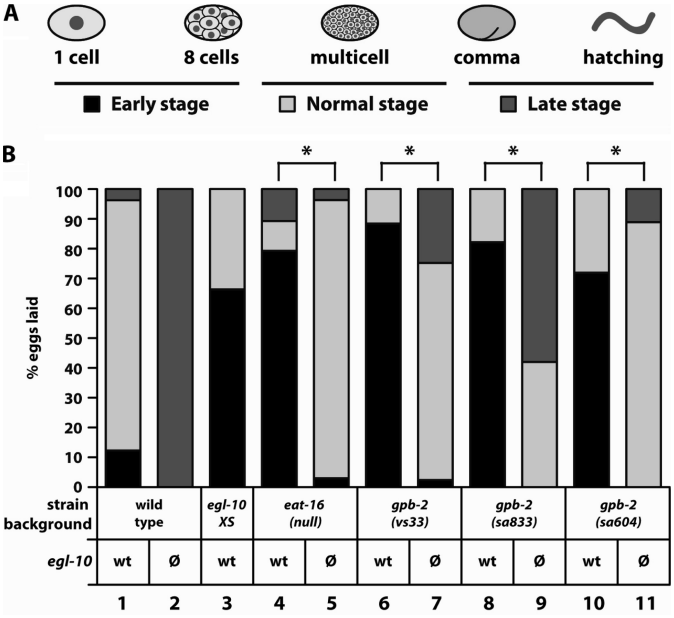

FIGURE 2. **Egg laying behavior of the indicated RGS and Gβ5 mutants ± *egl-10* null mutations.** *A, C. elegans* embryonic development indicating early, normal, and late stages for freshly laid eggs. *B,* percentage of eggs laid at each developmental stage by the indicated genotypes. *egl-10* XS indicates a strain carrying the *nls51* transgene that overexpresses EGL-10 from a transgene carrying multiple copies of the *egl-10* gene (17). *Asterisks* indicate significant differences ($p \leq 0.05$) between the percent of early stage eggs laid by bracketed strains. When *eat-16*(*null*) or *gpb-2*(*hyp*) mutations are combined with an *egl-10*(*null*) mutation, wild-type egg laying behavior is restored.

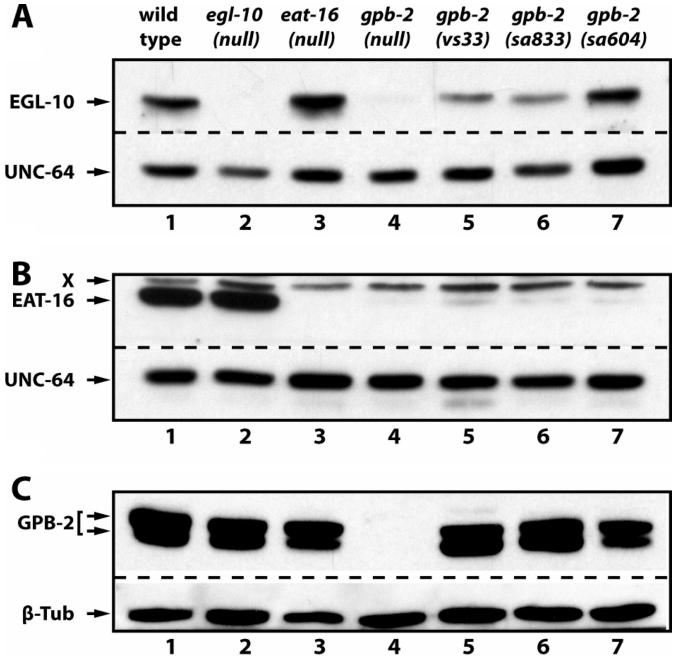

FIGURE 3. **Western analysis of EGL-10, EAT-16, and GPB-2 protein levels in whole worm lysates of the indicated genotypes.** EGL-10 runs just above 66 kDa; the EAT-16 antibody detects a single specific band just below 66 kDa, and a higher cross-reactive band (*X*), GPB-2 runs as a doublet at ~40 kDa; UNC-64 runs at ~33 kDa, and β-tubulin (*β-Tub*) runs at ~55 kDa. EAT-16 is virtually absent in all *gpb-2* mutants, whereas EGL-10 levels are higher in *gpb-2*(*hyp*) mutants than in the *gpb-2*(*null*).

We first observed the egg laying behavior of a number of control strains and classified the eggs laid by these animals as follows: early stage, less than eight cells; normal stage, nine cells to pre-comma; late-stage, comma and later (Fig. 2*A*). We found that the majority of eggs (84%) laid by wild-type animals were in the normal range of stages (Fig. 2*B*, *bar 1*), whereas 100% of eggs laid by *egl-10*(*null*) mutants, in which inhibitory $G\alpha_o$ signaling is increased, were of a late stage (Fig. 2*B*, *bar 2*). We next examined two hyperactive egg-laying mutants, an EGL-10-overexpressing strain, in which inhibitory $G\alpha_o$ signaling is strongly inhibited, and an *eat-16*(*null*) mutant in which stimulatory $G\alpha_q$ signaling is increased. We observed that both strains lay the majority of their eggs (66 and 79%, respectively) at early developmental stages (Fig. 2*B*, *bars 3* and *4*). Finally, we combined the hyperactive *eat-16*(*null*) mutation (too much $G\alpha_q$ signaling) with the *egl-10*(*null*) mutation (too much $G\alpha_o$ signaling), and as predicted we found these animals had a statistically significant decrease in the number of early stage eggs laid and now laid a majority (93%) of normal stage eggs (Fig. 2*B*, *bar 5*), similar to *gpb-2*(*null*) mutants and to wild-type animals.

Next, we put all three *gpb-2*(*hyp*) mutations through our genetic analysis. We found that all three single mutants laid the majority of their eggs at an early developmental stage as follows: *vs33*, 88%; *sa833*, 83%; *sa604*, 72% (Fig. 2*B*, *bars 6, 8,* and *10*). However, when combined with the *egl-10*(*null*) mutation, all three double mutants exhibited dramatic and statistically significant decreases in the number of early stage eggs laid, with *gpb-2*(*vs33*);*egl-10*(*null*) and *gbp-2*(*sa604*);*egl-10*(*null*) animals now laying the majority of their eggs, 73 and 89% respectively, within the normal range (Fig. 2*B*, *bars 7, 9* and *11*). This is consistent with *gpb-2*(*hyp*) mutations causing an increase in $G\alpha_q$ signaling and not a decrease in $G\alpha_o$ signaling.

EGL-10 and EAT-16 Levels Are Differentially Altered in gbp-2(hyp) Mutants—The increase in $G\alpha_q$ signaling could be explained by the *gpb-2*(*hyp*) mutations specifically decreasing activity of the inhibitor of $G\alpha_q$ signaling, EAT-16, rather than increasing the activity of the inhibitor of $G\alpha_o$ signaling, EGL-10. As both R7 RGS proteins require GPB-2/Gβ5 for stability, *gpb-2*(*hyp*) mutations might have this effect by specifically decreasing cellular EAT-16 levels. We investigated this possibility by analyzing the levels of EGL-10, EAT-16, and GPB-2/Gβ5 in whole worm lysates of wild-type, *gpb-2*(*null*), and *gpb-2*(*hyp*) animals. As expected, we found in our control experiments that each protein was present in wild-type animals and absent in the corresponding null mutants, confirming antibody specificity (Fig. 3, *A–C*, *lanes 1–4*). In addition, consistent with our previous data (9, 12), we observed that both EGL-10 and EAT-16 were virtually absent in *gpb-2*(*null*) mutants (Fig. 3, *A* and *B*, *lane 4*).

In contrast to *gpb-2*(*null*) mutants, all three *gpb-2*(*hyp*) mutant strains contained wild-type levels of GPB-2/Gβ5 protein (Fig. 3*C*, *lanes 5–7*) indicating that the *vs33*, *sa833,* and *sa604* point mutations do not destabilize the protein. We did, however, observe notable differences in the levels of EGL-10 and EAT-16. In all three *gpb-2*(*hyp*) mutants, we observed dramatic decreases in the level of EAT-16 protein similar to those seen in the null mutant (Fig. 3*B*, *lanes 5–7*). However all

three strains contained significantly more EGL-10 protein than did the *gpb-2*(*null*) animals. *gbp-2*(*vs33*) and *gpb-2*(*sa833*) contained intermediate levels of EGL-10 protein, whereas *gpb-2*(*sa604*) contained approximately wild-type levels of EGL-10 (Fig. 3*A*, *lanes 5–7*). Our results suggest *gpb-2*(*hyp*) mutations lead to greater decreases in EAT-16 levels than of EGL-10 levels, ultimately shifting the balance in favor of $G\alpha_q$ signaling relative to $G\alpha_o$ signaling.

gpb-2(hyp) Mutations Affect the Interface of GPB-2/Gβ5 with the DEP Domain of R7 RGS Proteins—We analyzed the position of each *gpb-2*(*hyp*) mutation within the R7 RGS·GPB-2·Gβ5 complex. We first aligned the sequence of *C. elegans* GPB-2 with that of the mouse Gβ5 protein, used in the published crystal structure of the RGS9-Gβ5 complex (13). As shown in Fig. 4*A* and supplemental Table 2, GPB-2/Gβ5 forms a seven WD40 repeat propeller, and all three *gpb-2*(*hyp*) mutations, *vs33* (D263Δ), *sa833* (C266Y), and *sa604* (D307N), affect conserved residues. When we mapped the *gpb-2*(*hyp*) mutations onto this structure, we found that the residues mutated in *vs33* and *sa833* are located within the fifth β-propeller blade, although the residue mutated in *sa604* is located nearby on blade six (Fig. 4*B*). Furthermore, we found that both the residues mutated in *vs33* and *sa604* are positioned at the interface with the R7 RGS DEP domain (Fig. 4*C*). These observations strongly suggest that the amino acids mutated in *gpb-2*(*vs33*) and *gpb-2*(*sa604*) play important roles in specifying the interaction of GPB-2/Gβ5 with either EAT-16 or EGL-10.

Homologous Interface Mutants of Mammalian Gβ5 Fail to Protect RGS9 and RGS7 from Proteolytic Degradation—Given the conservation of the Gβ5/R7 RGS interaction across species, we next asked whether the mutations at this interface have similar effects in the mammalian system. Based on the alignment between *C. elegans* GBP-2 and its mammalian homolog Gβ5, mutations at the corresponding positions in the mammalian Gβ5 short isoform (supplemental Table 2 D260A, C263Y, and D304N) were introduced by site-directed mutagenesis. We then checked the ability of these mutants to stabilize two representative mammalian R7 RGS proteins, RGS7 and RGS9. Consistent with published observations (34), co-transfection with Gβ5 in HEK293FT cells led to substantial stabilization of RGS7 as evidenced by the up-regulation of its levels (Fig. 5*A*). Unlike RGS7, association of Gβ5 with RGS9 is not sufficient to protect it from proteolytic degradation and additionally requires interaction with another binding partner, R7BP (10, 27). Consequently, we found that when co-transfected with R7BP, wild-type Gβ5 markedly enhanced the expression of RGS9 (Fig. 5*B*). In the presence of R7BP, the protection of RGS7 by wild-type Gβ5 was further increased. In contrast, neither D260A nor C263Y mutants of Gβ5 could enhance the expression of RGS7 and RGS9 in the absence or presence of R7BP. The third mutant D304N exerted effects similar to those of the wild-type Gβ5 suggesting that this mutation does not affect the stability of the complex. Importantly, the mutations did not seem to affect the expression levels of Gβ5 itself, analogous to our results with mutant GPB-2 proteins in *C. elegans* lysates (Fig. 3*C*), so the lack of R7 RGS stabilization by the D260A and C263Y mutants of Gβ5 cannot be explained by lower expression levels.

We next performed pulse-chase degradation experiments to determine whether the inability of the mutant Gβ5 constructs to enhance R7 RGS expression results from higher proteolytic susceptibility of the complexes (Fig. 5, *C* and *D*). Consistent with earlier reports (27, 34), we found that in the absence of Gβ5, both RGS7 (Fig. 5*C*) and RGS9 (Fig. 5*D*) have very short half-lives in cells (<1 h) due to high rates of proteolytic degradation (10, 27). Co-expression with wild-type Gβ5 increased the lifetime of both R7 RGS proteins by as much as 4–6-fold. However, when D260A or C263Y mutants were used instead of wild-type Gβ5, no increase in the lifetime of the RGS7 or RGS9 was evident (Fig. 5, *C* and *D*). Correlating with these results, we found that co-expression of wild-type Gβ5 largely protects RGS9 from ubiquitination, although the D260A and C263Y Gβ5 mutants failed to do so (supplemental Fig. 1). These data indicate that both D260A and C263Y mutants fail to provide proteolytic protection to RGS7 and RGS9 accounting for loss of their ability to support R7 RGS expression.

Intact Formation of RGS·Gβ5·R7BP Complexes with Gβ5 Mutants—Because Gβ5 directly binds to R7 RGS proteins (Fig. 6*A*), we next asked whether the loss of physical interaction could account for the inability of the Gβ5 mutants to provide proteolytic protection to the complexes. We first investigated the interaction between Gβ5 and full-length RGS9, as a representative R7 RGS protein, by co-immunoprecipitation. An AU5 epitope tag was appended to all Gβ5 constructs to discriminate them from endogenous Gβ5 present in HEK293 cells. As is evident from the data presented in Fig. 6*B*, wild-type Gβ5 as well as Gβ5-D260A and Gβ5-C263Y were co-immunoprecipitated by RGS9 antibodies. Similarly, reciprocal immunoprecipitation using anti-AU5 antibody pulled down readily detectable levels of RGS9 confirming the interaction (Fig. 6*C*). Lower binding levels observed with Gβ5 mutants match lower expression levels of these complexes and suggest that the mutations do not eliminate the interaction of Gβ5 with R7 RGS proteins.

The recently solved crystal structure of the RGS9·Gβ5 complex (13) reveals that Gβ5 binds to three sites in RGS9 (Fig. 6*A*). In addition to a coiled-coil interaction with the GGL domain, it also makes contacts with the DEP domain of RGS9, an interaction sufficiently robust to be detected by biochemical methods (35). The third rather limited point of contact is with the RGS domain. We therefore reasoned that if Gβ5 mutations affect interaction only at the DEP-binding interface, their effects could be masked when the binding is examined with RGS9 molecules in which the other binding interface remains intact. To investigate this possibility, we tested the binding of Gβ5 to either a DEP domain-containing N-terminal fragment (RGS9NT) or a GGL-containing C-terminal fragment (RGS9CT) separately. We found that both D260A and C263Y mutants could associate with RGS9NT or RGS9CT as well as did wild-type Gβ5, indicating the preservation of binding interactions at both sites.

Finally, we investigated the possibility that mutations in Gβ5 affect the ability of RGS9 to recruit R7BP, association

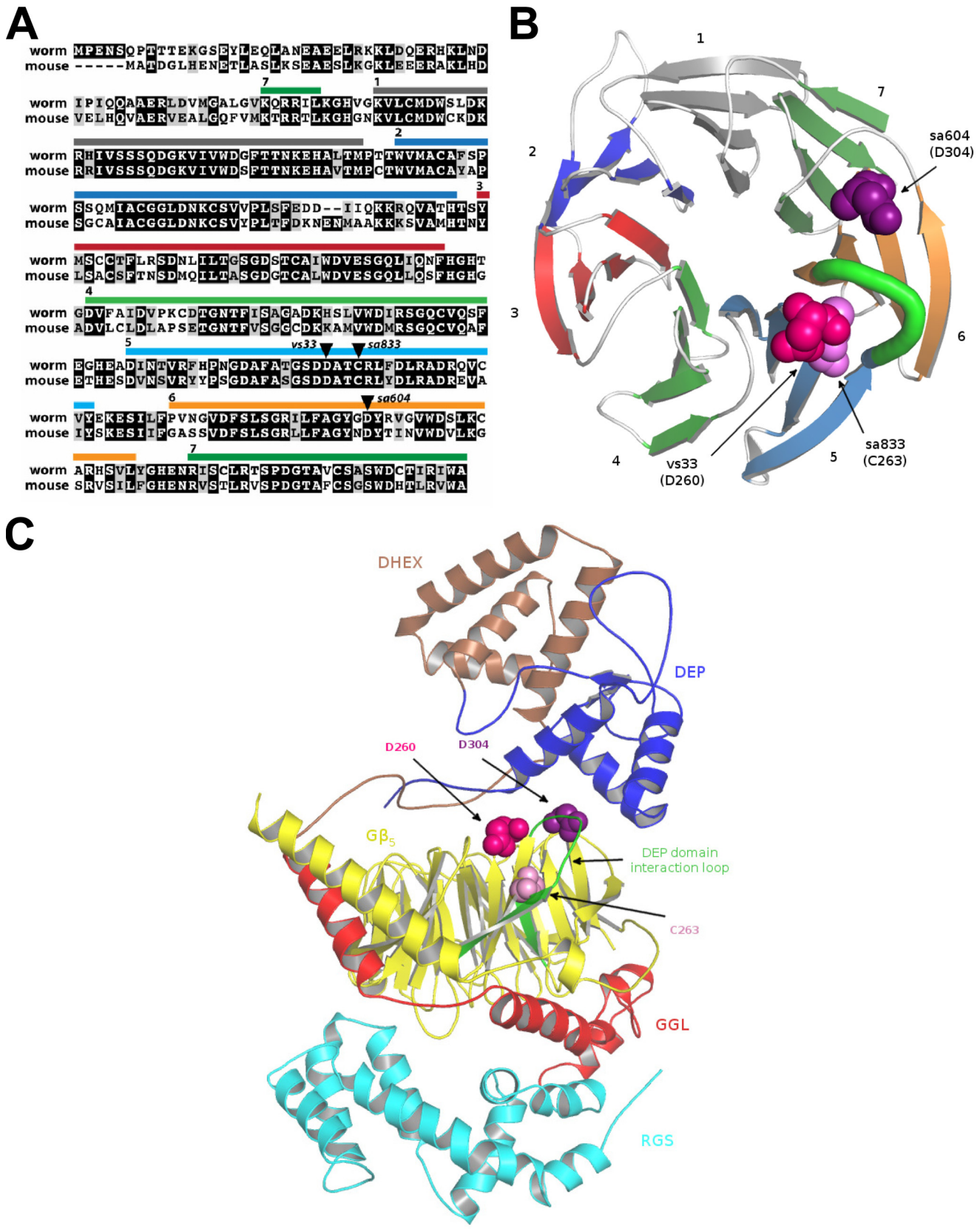

FIGURE 4. **Modeling of the residues mutated in *gpb-2*(*hyp*) mutations onto the crystal structure of mammalian RGS9·Gβ5.** *A*, alignment of *C. elegans* (worm) GPB-2 and mammalian (mouse) Gβ5. The location of each of the seven β-propellers in $G\beta_5$ and the Gβ5 amino acids corresponding to each *gpb-2*(*hyp*) mutation are indicated in *shades* of *purple*. *B*, location of the residues mutated in each *gpb-2*(*hyp*) mutation mapped on to the structure of $G\beta_5$ alone. *C*, mutated residues mapped on to the full structure of the RGS9·Gβ5 crystal structure. Individual domains of the RGS9 protein are indicated. Gβ5 loop connecting two β-strands (*green* in *B* and *C*) is engaged in extensive direct contacts with the DEP domain of RGS9.

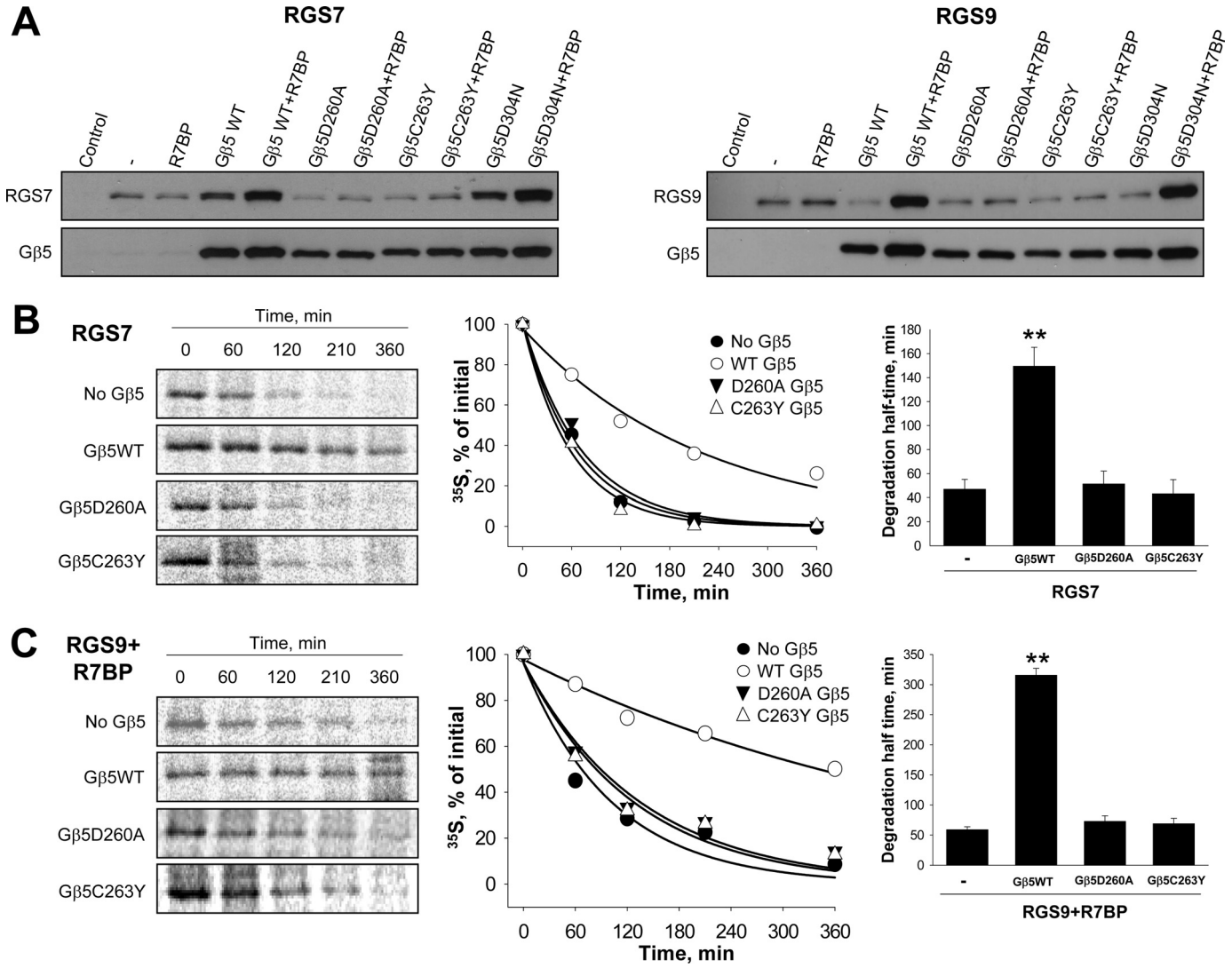

FIGURE 5. **Homologous interface mutations in mammalian Gβ5 lose the ability to protect R7 RGS proteins.** *A,* effects of Gβ5 constructs on the expression levels of RGS7 and RGS9 upon co-expression in mammalian HEK293 cells with and without R7BP. Lysates of the cells containing indicated proteins were resolved on SDS-PAGE and subjected to Western blotting using specific antibodies. *B,* measurement of RGS7 degradation rates by pulse-chase metabolic labeling. RGS7 was expressed in HEK293 cells alone or in combination with indicated Gβ5 constructs. *Left panel,* analysis of the timeline of ^{35}S-Met/Cys decay from the immunoprecipitated RGS7. Bands were visualized by autoradiography as described under "Experimental Procedures." Resulting band intensities were quantified and plotted as a function of time (*middle panel*). Single exponential fitting of each time course was used to determine protein half-lives in the cells, plotted as a *bar graph* (*right panel*). *C,* measurement of RGS9 degradation rates by pulse-chase metabolic labeling. The experiment was conducted as described for RGS7 in *B*. The data presented in the figure are representative of two to three independently conducted experiments. *Error bars* are S.E. *Double asterisks* denote $p < 0.01$, *t* test.

with which is also necessary for providing proteolytic protection to the complex (27). We obtained purified recombinant preparations of the RGS9·Gβ5WT, RGS9·Gβ5D260A, and RGS9·Gβ5C263Y complexes and studied their interactions with GST-tagged R7BP immobilized on the beads by pull-down assays. As shown in Fig. 6*F*, the ability of R7BP to effectively retain RGS9 was not detectably affected by the mutations in Gβ5. Together, these results demonstrate that mutations in Gβ5 destabilize RGS complexes by sensitizing them to proteolytic degradation without detectably affecting the initial formation of the trimeric R7 RGS·Gβ5·R7BP complexes.

Gβ5 Mutants Are Normally Processed by the CCTε·PhLP1 Chaperone Assembling Complex—The assembly of βγ complexes requires the assistance of the cytosolic chaperonin complex CCT, also known as TriC, which acts in cooperation with the co-chaperone phosducin-like protein 1 (PhLP1) to facilitate folding of β subunits (36). The crystal structure of the RGS9·Gβ5 complex revealed that the interaction of Gβ5 with the GGL domain of RGS9 shares the same organization as that seen in conventional βγ complexes (13). Furthermore, the protein interaction interface engaging in the interaction with phosducin-like proteins is also conserved in Gβ5 (13). Indeed, a recent study (37) has demonstrated that folding of Gβ5 and its assembly with R7 RGS proteins is mediated by the coordinated action of CCT and PhLP1 (Fig. 7*A*). These observations raise the possibility that mutations in Gβ5 compromise the stability of the complex by affecting how it is processed by the CCT-PhLP1 machinery. For example, the rate of complex assembly with RGS proteins would be

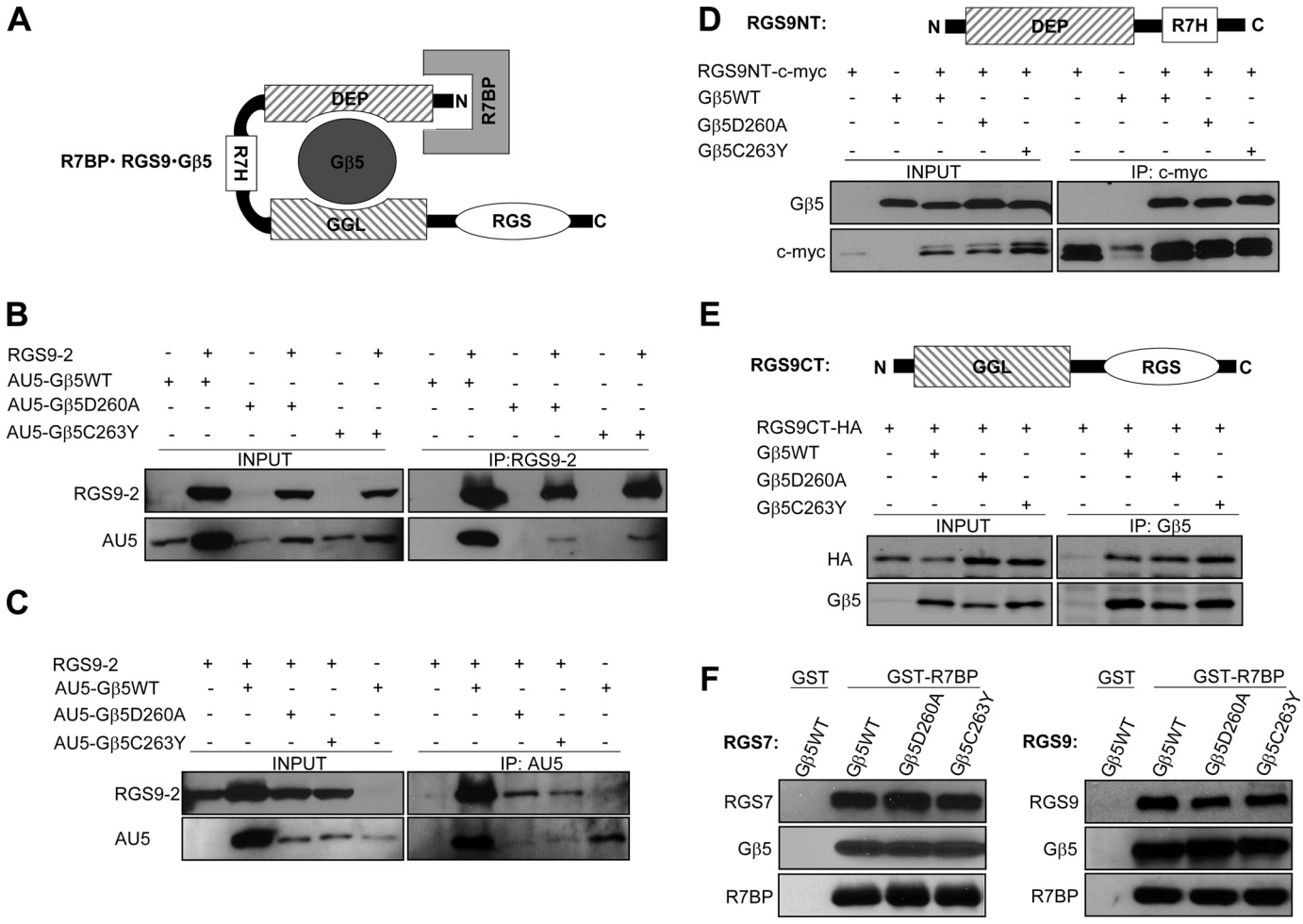

FIGURE 6. **Intact formation of RGS·Gβ5·R7BP complexes with Gβ5 mutants.** *A,* schematic diagram of the interactions within the RGS9·Gβ5·R7BP complex. Gβ5 binds to two domains in RGS9, the DEP domain and the GGL domain. Binding to R7BP, which is important for the proteolytic stability of the complex, is mediated by the DEP domain of RGS9. *B* and *C,* full-length RGS9 can associate with both wild-type and mutant Gβ5 subunits as shown by co-immunoprecipitation assays. Indicated constructs were co-transfected into HEK293 cells, and proteins were immunoprecipitated with antibodies against either RGS9 (forward immunoprecipitation, *B*) or the AU5 tag engineered in Gβ5 constructs (reverse immunoprecipitation (*IP*), *C*). *D* and *E,* mutations in Gβ5 do not detectably affect its binding to N- or C-terminal domains of RGS9. Indicated constructs containing either N-terminal (*D*) or C-terminal (*E*) fragments were separately co-transfected with wild-type or mutant Gβ5 in HEK293 cells, and interactions were followed by immunoprecipitation assays. The control (*C*) lanes shown indicate that the low levels of endogenous Gβ5 present in the HEK293 cells did not interfere with these assays. *F,* pulldown assays using recombinant GST-tagged R7BP show the interaction of full-length recombinant RGS9 bound to Gβ5 mutants is intact.

slowed if the interaction of Gβ5 with CCT and/or PhLP1 is disrupted.

We examined this possibility by comparing the association of wild-type and mutant Gβ5 proteins with PhLP1 and CCT complexes using immunoprecipitation assays. As shown in Fig. 7*B*, we detected no differences in the ability of wild-type Gβ5 and its D260A and C263Y mutants to interact with PhLP1 and CCT. We therefore concluded that Gβ5 mutants are normally processed by the CCT-PhLP1 machinery to form intact complexes with R7 RGS proteins.

Molecular Dynamic Simulations Show Substantial Re-arrangements of the DEP-Gβ5 Interface—Our biochemical observations indicate that the Gβ5 mutant retains its ability to associate with the R7 RGS proteins, suggesting subtle rearrangements in the complex that lead to its proteolytic destabilization. To gain insight into potential conformational changes in the RGS9·Gβ5 complex induced by the D260A and C263Y amino acid changes, we performed molecular dynamics (MD) simulation studies on the Gβ5 mutants structure alone and in complex with RGS9 (Fig. 8).

Analysis of the intermolecular interactions in the RGS9·Gβ5 complex using the EBI PISA server (38) indicates that Gβ5 forms a much weaker complex with the DEP domain (~8.4 kcal/mol solvation energy) as compared with the GGL domain (~32 kcal/mol). Both mutation sites reside in the β-turn loop that connects the second and third β-strands of the fifth blade of Gβ5 (Fig. 4*B*), and our analysis shows that the mutations leave the direct contacts of this mutated loop with the DEP domain intact. However, the mutated loop is adjacent to and contacts a "DEP domain interaction loop" that has much more significant interactions with the DEP domain (Fig. 8*A*), contributing about half of the contact surface of Gβ5 with the DEP domain and traversing the center of the binding epitope.

MD simulation of the mutant Gβ5 indicates that both mutations significantly influence the conformation of the DEP

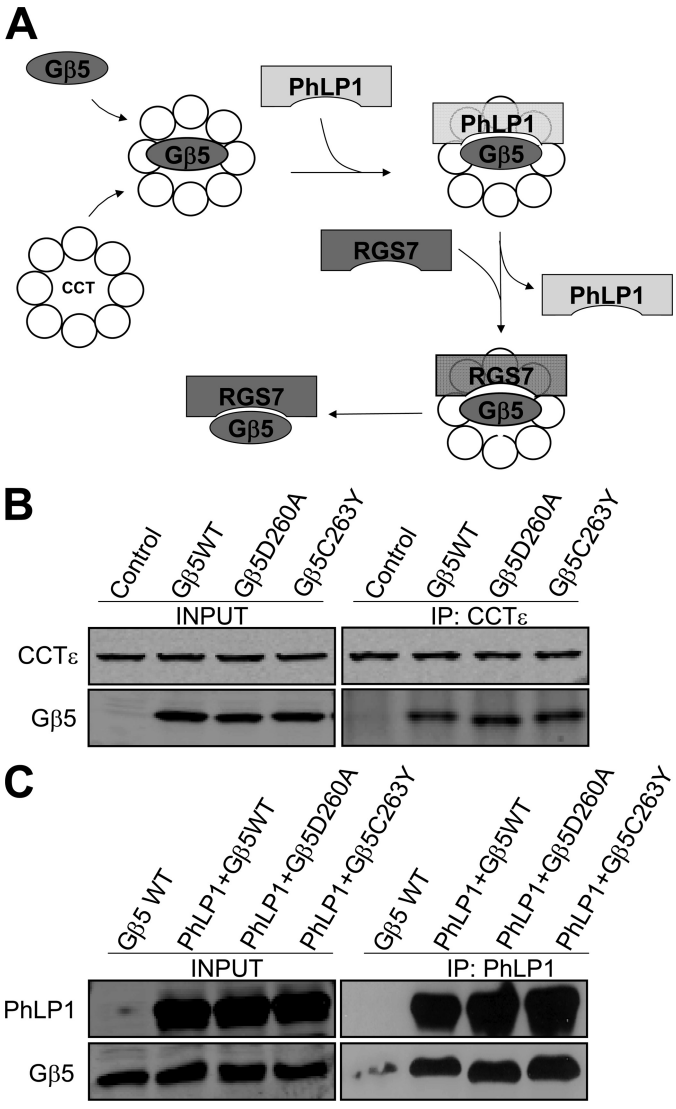

FIGURE 7. **Gβ5 mutants interact normally with the CCTε and PhLP1 assembling complex.** *A,* schematic diagram of the R7 RGS/Gβ5 assembly process. Gβ5 folding and assembly with RGS7 require assistance from CCT and PhLP1. Gβ5 is folded on chaperonin CCT, and the co-chaperon protein, PhLP1, binds to Gβ5 to stabilize the complex until Gβ5 is fully folded. *B,* wild-type and mutant Gβ5 co-immunoprecipitate with CCTε equally well. *C,* wild-type and mutant Gβ5 bind to PhLP1 with similar efficiency.

domain interaction loop. For example, D260A mutation converts the Asp-260 loop from a β-turn to a less tight α-turn (39). This conformational change may modify the backbone hydrogen bonding between the mutated loop and the DEP interaction loop, affecting the conformation of the Ile-283 and Phe-284, two key residues at the interface with the DEP domain (Fig. 8*B*). In the C263Y mutant, the mechanism affecting the DEP domain interaction loop is different, yet it leads to a similar disruption of the Ile-283/Phe-284 residues (Fig. 8*C*).

It thus appears that D260A and C263A mutations cause re-arrangement of the interface, perhaps by making the interactions more transient, without having large influence on the affinity of the DEP-Gβ5 binding. It needs to be noted that this MD simulation is not a direct experimental observation, and some deviations from these predictions are expected in the actual structure of the complex between Gβ5 mutants and RGS9. The major conclusion is instead that the D260A and C263Y mutations, although not located at the sites directly involved in forming the Gβ5/DEP interface, have the potential of significantly disrupting the conformation of the DEP/domain interaction loop and thus modulating the overall interaction.

DISCUSSION

In this study, we provide insights into the molecular mechanisms involved in post-translational control of R7 RGS protein expression. Volatility of R7 RGS expression in the nervous system is well documented. In neurons, the levels of RGS7 protein are up-regulated by stimulation of α_2-adrenergic (40), 5-HT2A (41), and TNFα1 (42) receptors. Similarly, levels of the best studied R7 RGS protein, RGS9, have been reported to change upon administration of addictive drugs such as cocaine (16), acute morphine (15), and amphetamine (43). Furthermore, alteration in striatal dopamine signaling in patients with Parkinson disease also lead to the elevation of RGS9 expression (14). We have recently reported that RGS9 expression is sensitive to changes in membrane potential and oxygenation (44). In several cases, it has now been documented that changes in R7 RGS protein levels occur as the result of regulated proteolytic degradation. For example, TNFα1 signaling up-regulates RGS7 levels by preventing proteasome-dependent degradation of RGS7 (42), and down-regulation of RGS9 protein levels occur as the result of rapid proteolytic degradation triggered by calcium entry (44). Increased susceptibility of R7 RGS proteins to proteolytic degradation has been shown to involve post-translational modifications such as ubiquitination (27, 42) and phosphorylation (42, 45) and/or recruitment of destabilizing factors such as the Hsc70 chaperone (46) that could serve to target RGS9 to lysosomal cysteine proteases for degradation (10). Thus, it appears that regulation of R7 RGS protein stability serves as a general mechanism by which neurons dynamically adjust the levels of these signaling molecules.

It is now well recognized that the stability of R7 RGS proteins requires their association with their binding partners R7BP (or its homolog R9AP) and Gβ5. Binding to R9AP or the homologous protein R7BP (RSBP-1 in *C. elegans*) is required for the stable expression of RGS9, RGS11, and EAT-16 (9, 28, 47). This regulation is rather selective because R9AP/R7BP/RSBP-1 do not influence the expression of RGS6, RGS7, and EGL-10. In contrast, complex formation with Gβ5 was found to be essential for the stability of all R7 RGS proteins, both in *C. elegans* (12) and mammals (11). Although this apparent hierarchical relationship suggests that Gβ5 is critical for the stability of R7 RGS proteins, it has remained unclear whether regulated association with Gβ5 has any role in the dynamic regulation of R7 RGS protein stability. The prevailing view has been that the association between R7 RGS and Gβ5 is constitutive in nature and that in the absence of Gβ5, GGL-containing RGS proteins simply fail to fold properly (48, 49) and are thus subject to destruction by the proteolytic systems that serve as the quality control checkpoint in the assembly of obligate oligomeric complexes. In this view, the Gβ5 and R7 RGS proteins are obligatorily and constitutively

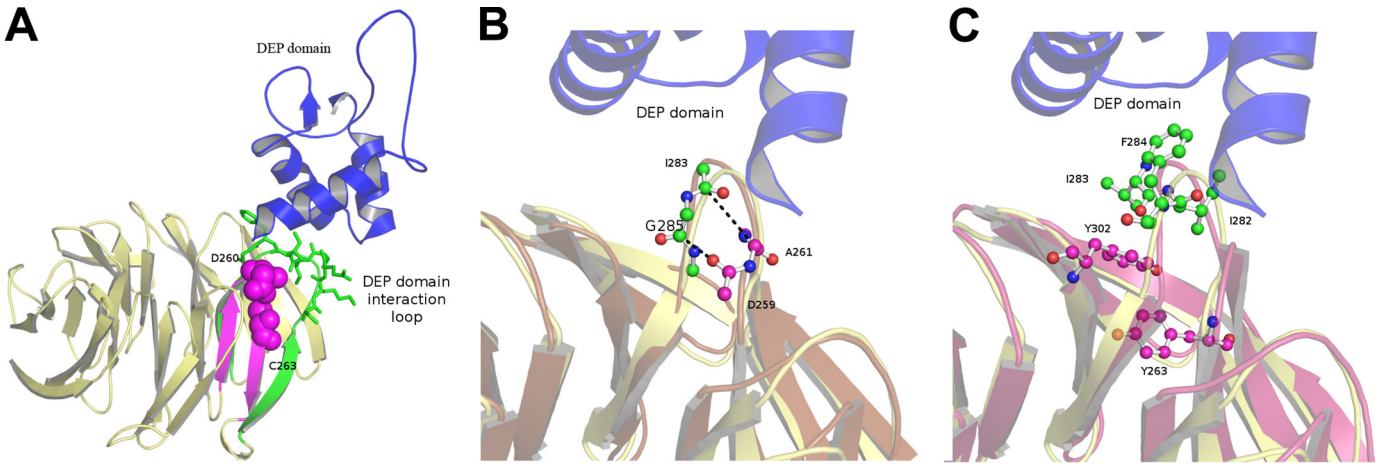

FIGURE 8. **Conformational changes in D260A and C263Y Gβ5 mutants predicted by molecular dynamics simulations.** *A,* detailed view of the DEP domain interaction with Gβ5. The DEP domain of RGS9 is shown in *cyan*. Gβ5 is colored in *pale yellow* with the "DEP domain interaction loop" (connecting the fourth β-strand of the sixth propeller blade and first β-strand of the seventh blade; amino acids Lys-279 through Gly-285) and the β-strands that it connects shown in *green*. The side chains of amino acids involved in the interaction with the DEP domain are indicated by *stick models*. The loop that contains mutations and the β-strands that it connects are highlighted in *pink*. Mutated residues (Asp-260 and Cys-263) are shown with space-filling models. *B,* predicted conformational changes in the DEP domain interaction loop induced by the D260A mutation in Gβ5. The backbone for the wild-type Gβ5 is depicted in *pale yellow* and the predicted mutant structure from MD simulations in *brown*. *Green balls* indicate the position of carbon atoms of the labeled amino acid residues in the DEP domain interaction loop, and *pink balls* designate the position of carbons in amino acids of labeled residues in the adjacent mutated loop. *Dashed lines* indicate new hydrogen bonds in the D260A mutant predicted by MD simulation. *C,* predicted conformational changes in the DEP domain interaction loop of Gβ5 upon C263Y mutation. The backbone of the wild-type Gβ5 is depicted in *pale yellow* and the predicted structure from MD simulations in *light pink*. *Green balls* indicate the position of carbon atoms of the labeled amino acid residues in the DEP domain interaction loop, *pink balls* designate the position of carbons in the mutant residue Tyr-263, and in the Tyr-302 residue whose position is displaced. More detailed information regarding changes observed upon MD simulations can be obtained by analyzing PyMOL session files and Protein Data Bank coordinates of Gβ5 mutants at the end point of the simulations that are available as supplemental material.

associated in exactly the same manner as conventional G protein β and γ subunits, with these associations depending on analogous coiled-coil interactions between Gβ5 and the GGL domain of R7 RGS, or the conventional Gβ and Gγ subunits, respectively. In this study, we challenge this view by demonstrating in both *C. elegans* and mammals that association of the GGL domain with Gβ5 is not sufficient for providing proteolytic protection to the R7 RGS complexes. We identified and characterized specific point mutations in Gβ5 that do not affect the coiled-coil interaction with the GGL domain and do not affect Gβ5 assembly into complexes with R7 RGS and R7BP proteins, but they do nevertheless abolish the proteolytic stabilization that normally results from the interaction by perturbing the Gβ5-DEP interface.

From unbiased genetic screens for *C. elegans* mutants with the hyperactive phenotype characteristic of increased $G\alpha_q$ signaling, we identified and characterized three independent mutations in *C. elegans* Gβ5 that result in degradation of the EAT-16 R7 RGS protein that inhibits $G\alpha_q$. These screens selected for a very special class of Gβ5 mutations, because seeing the hyperactive phenotype requires that the mutant Gβ5 retains the ability to form a functional complex with the second R7 RGS protein in *C. elegans*, EGL-10. Our Western analysis shows that two of the three mutations selected also partially destabilized EGL-10, just not to the same extent that they destabilized EAT-16.

The special Gβ5 mutations selected in the *C. elegans* genetic screens affect the conformation of the so-called "protein interaction" interface in Gβ5 (50, 51). This surface is formed by the loops connecting individual WD-40 repeat units. Interestingly, the analogous surface in conventional Gβ subunits serves as a critical contact point that mediates βγ interactions with most of its partners, including α subunits (52, 53), effectors (51), and regulatory proteins, *e.g.* phosducin (54). Moreover, analysis of the RGS9-Gβ5 crystal structure indicates that many of the key residues involved in these interactions are also conserved in Gβ5 but are instead involved in binding to the DEP domain of RGS9 (13). The interactions of conventional Gβ subunits via the protein interaction interface are all reversible binding interactions in which Gβ is required to repeatedly bind and then dissociate from its partners as signaling is initiated or terminated. Our modeling of the Gβ5/DEP interaction suggests a relatively weak binding interface that would similarly allow binding at this interface to be reversible, raising the possibility that R7 RGS complexes undergo conformational rearrangements in which this interface opens up. Indeed, Narayanan *et al.* (35) used several lines of biochemical evidence to show that the Gβ5-DEP association within the Gβ5·RGS7 complex is dynamic and adopts both open and closed conformations. Rearranging the conformation of the Gβ5-DEP interface likely exposes otherwise masked instability determinants contained within the DEP domain.

In addition to engaging in the interaction with Gβ5, the DEP domain of R7 RGS proteins also mediates binding to the membrane-targeting subunits R9AP/R7BP/RSBP-1, an interaction that can also affect stability of the complex (9, 30, 55, 56). Given that R9AP/R7BP/RSBP-1 protect only some R7 RGS members from proteolysis (10, 27) and that all R7 RGS proteins as well as R7BP are severely destabilized when Gβ5 is eliminated (10, 11, 57), we propose a model in which the primary stabilizing effect is provided by the interaction of Gβ5 with the DEP domain. The unique organization of the DEP interface of the "unstable" R7 RGS proteins (RGS9, RGS11, and EAT-16) might not allow Gβ5 to fully engage in the inter-

action without the assistance of R9AP/R7BP/RSBP-1, whose function might be to merely modulate the Gβ5/DEP interaction. Indeed, in biochemical experiments using stringent wash conditions, Gβ5 binds to the DEP domain of RGS7 but not to that of RGS9 (35). Consistent with this model, mutations destabilizing the Gβ5-DEP interface in *C. elegans* appear to have more pronounced effects on the stability of the R7 RGS protein EAT-16 that requires assistance from R7BP/RSBP-1. This phenomenon led to the imbalance between EAT-16 and EGL-10 protein levels that allowed us to identify Gβ5/DEP interaction mutations in the first place.

The results of our study allows us to conclude that the Gβ5-DEP interface of the R7 RGS complexes is a conserved "hot spot" that is critically involved in setting the stability of R7 RGS complexes to proteolytic degradation. It prompts speculation that a range of signaling events known to modulate R7 RGS function and protein levels do so at least in part by affecting the Gβ5-DEP interface through conformational changes, post-translational modifications, or the recruitment of various host factors.

Acknowledgments—We thank Dr. William Simonds (NIDDK, National Institutes of Health) for the gift of anti-RGS7 and anti-Gβ5 antibodies, Dr. Barry Willardson (Brigham Young University) for providing PhLP1 expression construct, Dr. Mike Nonet (Washington University) for the anti-UNC-64 antibody, and Dr. Jim Thomas (University of Washington) for the sa833 and sa604 mutants of gpb-2.

REFERENCES

1. Wettschureck, N., and Offermanns, S. (2005) *Physiol. Rev.* **85,** 1159–1204
2. Wilkie, T. M. (2000) *Curr. Biol.* **10,** R853–R856
3. Hollinger, S., and Hepler, J. R. (2002) *Pharmacol. Rev.* **54,** 527–559
4. Ross, E. M., and Wilkie, T. M. (2000) *Annu. Rev. Biochem.* **69,** 795–827
5. Bastiani, C., and Mendel, J. (2006) Heterotrimeric G Proteins in *C. elegans* (WormBook, ed) The *C. elegans* Research Community, WormBook, doi/10.1895/wormbook.1.75.1
6. Porter, M. Y., and Koelle, M. R. (2009) *Prog. Mol. Biol. Transl. Sci.* **86,** 15–47
7. Anderson, G. R., Posokhova, E., and Martemyanov, K. A. (2009) *Cell Biochem. Biophys.* **54,** 33–46
8. Traynor, J. R., Terzi, D., Caldarone, B. J., and Zachariou, V. (2009) *Trends Pharmacol. Sci.* **30,** 105–111
9. Porter, M. Y., and Koelle, M. R. (2010) *Mol. Biol. Cell.* **21,** 232–243
10. Anderson, G. R., Lujan, R., Semenov, A., Pravetoni, M., Posokhova, E. N., Song, J. H., Uversky, V., Chen, C. K., Wickman, K., and Martemyanov, K. A. (2007) *J. Neurosci.* **27,** 14117–14127
11. Chen, C. K., Eversole-Cire, P., Zhang, H., Mancino, V., Chen, Y. J., He, W., Wensel, T. G., and Simon, M. I. (2003) *Proc. Natl. Acad. Sci. U.S.A.* **100,** 6604–6609
12. Chase, D. L., Patikoglou, G. A., and Koelle, M. R. (2001) *Curr. Biol.* **11,** 222–231
13. Cheever, M. L., Snyder, J. T., Gershburg, S., Siderovski, D. P., Harden, T. K., and Sondek, J. (2008) *Nat. Struct. Mol. Biol.* **15,** 155–162
14. Tekumalla, P. K., Calon, F., Rahman, Z., Birdi, S., Rajput, A. H., Hornykiewicz, O., Di Paolo, T., Bédard, P. J., and Nestler, E. J. (2001) *Biol. Psychiatry* **50,** 813–816
15. Zachariou, V., Georgescu, D., Sanchez, N., Rahman, Z., DiLeone, R., Berton, O., Neve, R. L., Sim-Selley, L. J., Selley, D. E., Gold, S. J., and Nestler, E. J. (2003) *Proc. Natl. Acad. Sci. U.S.A.* **100,** 13656–13661
16. Rahman, Z., Schwarz, J., Gold, S. J., Zachariou, V., Wein, M. N., Choi, K. H., Kovoor, A., Chen, C. K., DiLeone, R. J., Schwarz, S. C., Selley, D. E., Sim-Selley, L. J., Barrot, M., Luedtke, R. R., Self, D., Neve, R. L., Lester, H. A., Simon, M. I., and Nestler, E. J. (2003) *Neuron* **38,** 941–952
17. Koelle, M. R., and Horvitz, H. R. (1996) *Cell* **84,** 115–125
18. Krispel, C. M., Chen, D., Melling, N., Chen, Y. J., Martemyanov, K. A., Quillinan, N., Arshavsky, V. Y., Wensel, T. G., Chen, C. K., and Burns, M. E. (2006) *Neuron* **51,** 409–416
19. Anderson, G. R., Cao, Y., Davidson, S., Truong, H. V., Pravetoni, M., Thomas, M. J., Wickman, K., Giesler, G. J., Jr., and Martemyanov, K. A. (2010) *Neuropsychopharmacology* **35,** 1040–1050
20. Robatzek, M., Niacaris, T., Steger, K., Avery, L., and Thomas, J. H. (2001) *Curr. Biol.* **11,** 288–293
21. Robatzek, M., and Thomas, J. H. (2000) *Genetics* **156,** 1069–1082
22. Brenner, S. (1974) *Genetics* **77,** 71–94
23. Bany, I. A. (2004) *Genetic and Cellular Analysis of the Inhibition of Egg Laying in Caenorhabditis elegans*, Ph.D. thesis, Yale University, New Haven, CT
24. Jose, A. M., Bany, I. A., Chase, D. L., and Koelle, M. R. (2007) *Genetics* **175,** 93–105
25. Wicks, S. R., Yeh, R. T., Gish, W. R., Waterston, R. H., and Plasterk, R. H. (2001) *Nat. Genet.* **28,** 160–164
26. Chase, D. L., and Koelle, M. R. (2004) *Methods Enzymol.* **389,** 305–320
27. Anderson, G. R., Semenov, A., Song, J. H., and Martemyanov, K. A. (2007) *J. Biol. Chem.* **282,** 4772–4781
28. Cao, Y., Masuho, I., Okawa, H., Xie, K., Asami, J., Kammermeier, P. J., Maddox, D. M., Furukawa, T., Inoue, T., Sampath, A. P., and Martemyanov, K. A. (2009) *J. Neurosci.* **29,** 9301–9313
29. Skiba, N. P., Martemyanov, K. A., Elfenbein, A., Hopp, J. A., Bohm, A., Simonds, W. F., and Arshavsky, V. Y. (2001) *J. Biol. Chem.* **276,** 37365–37372
30. Martemyanov, K. A., Yoo, P. J., Skiba, N. P., and Arshavsky, V. Y. (2005) *J. Biol. Chem.* **280,** 5133–5136
31. Hess, B. C., Kutzner, D., van der Spoel, and Lindahl, E. (2008) *J. Chem. Theor. Comput.* **4** 435–447
32. van der Linden, A. M., Simmer, F., Cuppen, E., and Plasterk, R. H. (2001) *Genetics* **158,** 221–235
33. Ranganathan, R., Cannon, S. C., and Horvitz, H. R. (2000) *Nature* **408,** 470–475
34. Witherow, D. S., Wang, Q., Levay, K., Cabrera, J. L., Chen, J., Willars, G. B., and Slepak, V. Z. (2000) *J. Biol. Chem.* **275,** 24872–24880
35. Narayanan, V., Sandiford, S. L., Wang, Q., Keren-Raifman, T., Levay, K., and Slepak, V. Z. (2007) *Biochemistry* **46,** 6859–6870
36. Willardson, B. M., and Howlett, A. C. (2007) *Cell. Signal.* **19,** 2417–2427
37. Howlett, A. C., Gray, A. J., Hunter, J. M., and Willardson, B. M. (2009) *J. Biol. Chem.* **284,** 16386–16399
38. Krissinel, E., and Henrick, K. (2007) *J. Mol. Biol.* **372,** 774–797
39. Chou, K. C. (2000) *Anal. Biochem.* **286,** 1–16
40. Jedema, H. P., Gold, S. J., Gonzalez-Burgos, G., Sved, A. F., Tobe, B. J., Wensel, T., and Grace, A. A. (2008) *Eur. J. Neurosci.* **27,** 2433–2443
41. Singh, R. K., Shi, J., Zemaitaitis, B. W., and Muma, N. A. (2007) *J. Pharmacol. Exp. Ther.* **322,** 133–140
42. Benzing, T., Brandes, R., Sellin, L., Schermer, B., Lecker, S., Walz, G., and Kim, E. (1999) *Nat. Med.* **5,** 913–918
43. Burchett, S. A., Volk, M. L., Bannon, M. J., and Granneman, J. G. (1998) *J. Neurochem.* **70,** 2216–2219
44. Anderson, G. R., Lujan, R., and Martemyanov, K. A. (2009) *Mol. Cell. Biol.* **29,** 3033–3044
45. Benzing, T., Köttgen, M., Johnson, M., Schermer, B., Zentgraf, H., Walz, G., and Kim, E. (2002) *J. Biol. Chem.* **277,** 32954–32962
46. Posokhova, E., Uversky, V., and Martemyanov, K. A. (2010) *J. Proteome Res.* **9,** 1510–1521
47. Keresztes, G., Martemyanov, K. A., Krispel, C. M., Mutai, H., Yoo, P. J., Maison, S. F., Burns, M. E., Arshavsky, V. Y., and Heller, S. (2004) *J. Biol. Chem.* **279,** 1581–1584
48. Sondek, J., and Siderovski, D. P. (2001) *Biochem. Pharmacol.* **61,** 1329–1337
49. Jones, M. B., Siderovski, D. P., and Hooks, S. B. (2004) *Mol. Interv.* **4,** 200–214

50. Smrcka, A. V. (2008) *Cell. Mol. Life Sci.* **65,** 2191–2214
51. Ford, C. E., Skiba, N. P., Bae, H., Daaka, Y., Reuveny, E., Shekter, L. R., Rosal, R., Weng, G., Yang, C. S., Iyengar, R., Miller, R. J., Jan, L. Y., Lefkowitz, R. J., and Hamm, H. E. (1998) *Science* **280,** 1271–1274
52. Wall, M. A., Coleman, D. E., Lee, E., Iñiguez-Lluhi, J. A., Posner, B. A., Gilman, A. G., and Sprang, S. R. (1995) *Cell* **83,** 1047–1058
53. Sondek, J., Bohm, A., Lambright, D. G., Hamm, H. E., and Sigler, P. B. (1996) *Nature* **379,** 369–374
54. Gaudet, R., Bohm, A., and Sigler, P. B. (1996) *Cell* **87,** 577–588
55. Hu, G., Zhang, Z., and Wensel, T. G. (2003) *J. Biol. Chem.* **278,** 14550–14554
56. Martemyanov, K. A., Lishko, P. V., Calero, N., Keresztes, G., Sokolov, M., Strissel, K. J., Leskov, I. B., Hopp, J. A., Kolesnikov, A. V., Chen, C. K., Lem, J., Heller, S., Burns, M. E., and Arshavsky, V. Y. (2003) *J. Neurosci.* **23,** 10175–10181
57. Grabowska, D., Jayaraman, M., Kaltenbronn, K. M., Sandiford, S. L., Wang, Q., Jenkins, S., Slepak, V. Z., Smith, Y., and Blumer, K. J. (2008) *Neuroscience* **151,** 969–982